Originally published as:

"13.17 Oxidative Coupling of Methane"
E. V. Kondratenko, M. Baerns
In: Handbook of Heterogeneous Catalysis, Vol. **6**, (2008) 3010-3023

ISBN-Nummer: 978-3-527-31241-2

Reprint from

Handbook of Heterogeneous Catalysis

8 Volumes

Edited by
Gerhard Ertl, Helmut Knözinger, Ferdi Schüth,
and Jens Weitkamp

Second, Completely Revised and Enlarged Edition

WILEY-
VCH

13.17
Oxidative Coupling of Methane

*Evgenii V. Kondratenko and Manfred Baerns**

13.17.1
Introduction

Methane is the main constituent of natural gas, the reserves of which are estimated to exceed those of crude oil in the future. Therefore, a strong economic interest exists in developing processes that allow methane conversion to higher valued products. Currently, methane is industrially converted to syngas via steam reforming [1] and to hydrocyanic acid via the Andrussow [2] or Degussa processes [2]. The oxidative coupling of methane (OCM) to ethane and ethene is an attractive alternative for the existing processes based on crude oil. Most of the research and development work on the highly exothermic catalytic OCM reaction started in the early 1980s [3–5]. The progress of this work is the subject of the present chapter, which covers roughly the last 10–15 years; for earlier work the reader is referred to various comprehensive reviews [6a, 7–9]. It is certainly worth mentioning that the highly endothermic pyrolysis of methane to acetylene and partly to ethylene had been already developed and put into practice in the 1930s using an electric arc (Hüls [10]) or partial combustion of methane (BASF [10]) as a source of heat for the highly endothermic pyrolysis reaction.

This chapter deals specifically with the progress made in the fundamental understanding of OCM, new methods and working hypotheses in the design of novel catalysts and their required properties (e.g. role of structural defects and electronic properties). Attention is also paid to reaction and process engineering; this comprises reaction kinetics, novel catalytic reactors and their operation, modeling and simulation and, finally, novel process engineering concepts.

13.17.2
Fundamentals of the OCM Reaction

13.17.2.1 Catalytic Materials and Their Performance

Since the pioneering works of Keller and Bhasin [3] and Hinsen and Baerns [4], a large number of different catalytic materials (supported and non-supported) have been investigated for the OCM reaction. The aim was to achieve high selectivities towards C_2 products (C_2H_4 and C_2H_6) at methane conversions as high as possible. The most convenient systematization of the studied materials has been given by Lee and Oyama [11] and later by other groups [6, 7, 12]. All the catalytic materials known were divided into four groups: (i) reducible metal oxides, (ii) non-reducible metal oxides, (iii) halogen-containing oxide materials and (iv) solid electrolytes.

Catalysts in the first group are required for the so-called redox OCM operation using alternating (periodic) feeds of methane and oxygen. C_2 products are formed via methane oxidation by oxygen from the catalyst in the methane period. The reduced catalyst is reoxidized in the oxygen cycle. An advantage of this mode of operation is the elimination of the expensive separation of oxygen from air, since catalyst reoxidation is performed with air. In pioneering work at Atlantic Richfield [13], $NaMnO_4/MgO–SiO_2$ and Mn_3O_4 were identified as suitable catalytic systems. However, a low productivity was achieved due to the short time (ca. 2 min) of operation during OCM and the long time interval (130 min) for reoxidation of the reduced catalytic material. The catalytic performance was later improved by catalyst modification [14, 15]. Recently, Mn- and Co-based perovskites were identified as effective catalysts for the OCM reaction using alternating feeds of methane and oxygen [16]. A C_2 yield of 20% was obtained over $SrCoO_3$ doped with the oxides or hydroxides of K and Na; the reactor was operated at 1073 K, applying a 1.5-min cycle of methane. However, the catalyst productivity still remained low. For the realization of the OCM reaction in

* Corresponding author.

Tab. 1 OCM performance over selected catalytic materials

Catalyst	T/K	$p(CH_4)$/kPa	$p(O_2)$/kPa	P_{total}/kPa	$X(CH_4)$/%	$S(C_2)^a$/%	$Y(C_2)^b$/%	Ref.
Li/MgO	1013	10	5	100	37.8	50.3	19	[17]
30% BaO/Ga_2O_3	1023	16.8	6.8	100	32	54	17.3	[18]
95 mol% BaF_2/Y_2O_3	1023	16.8	6.8	100	36.1	62.1	22.4	[19]
La/MgO	1073	80	20	100	29.3	58.8	17.2	[20]
Rb_2WO_4/SiO_2	1123	82	18	100	32	78	25	[21]
$Bi_{1.5}Y_{0.3}Sm_{0.2}O_{3-\delta}$	1223	33.3	16.6	100	43.5	62	27	[22]
$La_2O_3-CeO_2$	1048	83.6	16.4	100	22.3	66	14.7	[23]
Na_2WO_4/SiO_2	1123	82	18	100	44	52	22.9	[21]
Sm_2O_3	1053	87.4	12.6	100	20	65.4	13.1	[23]

[a] $S(C_2)$ = selectivity towards C_2H_6 and C_2H_4.
[b] $Y(C_2)$ = yield of C_2H_6 and C_2H_4.

such a mode of operation, the following requirements are important:

(i) high catalyst stability under reducing and oxidizing conditions at high temperatures
(ii) catalyst ability to offer a high amount of lattice oxygen for the oxidation reaction
(iii) minimal time of catalyst reoxidation in comparison with that of the OCM reaction.

In contrast to reducible metal oxides, non-reducible metal oxides show low activity in the periodic mode of operation but perform well in the co-feed mode, where methane and oxygen are simultaneously fed. Selected well-performing catalytic materials are listed in Table 1. The catalytic materials based on oxides of rare earth and alkaline earth metals belong to the best performing types. Promotion of these materials and also of reducible oxides with alkaline earth and alkali metal oxides enhances their C_2 selectivities significantly. The promoting effect of dopants on the catalytic performance of various oxides is discussed in Section 13.17.2.3. From Table 1, it can be clearly seen that the yield of C_2 hydrocarbons does not exceed 30%, which is in agreement with the "upper-bound" calculations referred to in Section 13.17.2.5.

Anshits and coworkers [24–26] developed novel micro-designed catalytic materials for the OCM reaction. The catalysts are magnetic crystalline microspheres and cenospheres recovered from fuel ash. They consist of calcium aluminosilicate ($CaO-Al_2O_3-2SiO_2$) as a binding material and of α-Fe_2O_3 and a solid solution consisting of Fe_3O_4 and Mg(Mn)-ferrite being the active components. Catalyst treatment with HF resulted in stabilization of Fe_3O_4 and simultaneous improvement of catalytic performance. A C_2 yield of 16% was achieved at 1123 K using a non-diluted CH_4-O_2 (85:15) feed.

Halogen-containing oxide materials show a high selectivity towards C_2 hydrocarbons at a high level of methane conversion. In their pioneering work, Otsuka et al. [27] reported a significant improvement in catalytic performance of manganese oxide when it was promoted with lithium chloride. A yield of C_2 hydrocarbons of ca. 31% was achieved at 1023 K. Many later papers [28–31] described the improvement of the catalytic performance of various oxides by doping with chlorides. It is also important to note that not only solid promoters but also gaseous chloride-containing compounds enhanced the OCM performance. The effect of chlorides was explained by chlorine generation, which initiates gas-phase reactions. A recent patent [32] claimed an ethene yield of ca. 30% over a perovskite catalyst compossed of $BaO \cdot TiO_2 + SnCl_2$ of different proportions at 1048 K using a non-diluted CH_4-O_2 (2:1) mixture. However, the high catalytic performance decreased with time-on-stream due to the loss of chlorine. The catalyst stability could be improved by injecting carbon tetrachloride into the reaction feed. Au et al. [19] reported that methane is selectively converted to C_2 hydrocarbons over 95 mol% BaF_2/Y_2O_3 catalyst. A C_2 yield of ca. 22.5% was achieved at 1023 K, whereas non-doped Y_2O_3 performed less selectively (C_2 yield $\approx$ 8%). The improving effect of BaF_2 was ascribed to the creation of structural defects, which were considered to be essential for generating active oxygen species.

At the end of the 1980s, Machida and Enyo [33] reported a C_2 yield of 31.6% at 1023 K over an $SrCe_{0.9}Yb_{0.1}O_{3-x}$ solid electrolyte. The high catalytic performance was related to the proton conductivity of the catalyst. Several later papers dealt with the application of solid electrolytes for the OCM reaction in membrane reactors and have been reviewed [34, 35].

13.17.2.2 Mechanistic Aspects

The OCM reaction usually occurs via a heterogeneous–homogeneous mechanism, i.e. the

References see page 3021

reaction is initiated on the catalyst surface by the generation of methyl radicals and continues in the gas phase. Lunsford and coworkers [36, 37] observed methyl radicals by means of matrix isolation electron spin resonance (ESR) over various catalytic materials. Buyevskaya et al. [38] proved the formation of gas-phase methyl radicals via heterogeneous reaction of methane with adsorbed oxygen species over MgO and Sm_2O_3 under Knudsen diffusion conditions using a temporal analysis of products (TAP) reactor. Hence there is no doubt that the cleavage of one C–H bond of the methane molecule is a crucial step of the OCM reaction. However, there were two different points of view on the mechanism, i.e. heterolytic or homolytic breaking the C–H bond. According to the former concept, CH_3^- and H^+ are formed upon activation of the C–H bond [Eq. (1)] followed by the transformation of the methyl anion formed into a methyl radical [Eq. (2)]. Methyl radicals are formed directly from methane by homolytic splitting of the C–H bond [Eq. (3)]. The idea of heterolytic breaking of the C–H bond is based on the well-established experimental observation that selective catalytic materials are of basic nature [6b, 7, 12]. A correlation between the concentration of basic sites and the rates of C_2 products formation was established over oxides and phosphates of alkaline earth metals [39] and Pb/MgO [40]. However, this correlation cannot be generalized for all known catalytic materials for the OCM reaction.

$$CH_4 + M^{n+}O^{2-} \longrightarrow M^{n+}CH_3^- + O^{2-}H^+ \quad (1)$$

$$M^{n+}CH_3^- \xrightarrow{e} CH_3^\bullet \quad (2)$$

$$CH_4 + (O)_s \longrightarrow CH_3^\bullet + (OH)_s \quad (3)$$

Since methyl radicals are products of methane activation via both heterolytic and/or homolytic breaking of the C–H bond, their presence in the gas phase cannot be considered as unambiguous evidence for one of the concepts. Therefore, the two mechanistic concepts were discriminated by H–D isotopic exchange in the CH_4 molecule as reported by many authors [40–43]. The isotopic exchange is assumed to proceed on basic sites via an anionic intermediate, i.e. heterolytic breaking. Nelson et al. [41] determined very low activity of an Li/MgO catalyst for H–D exchange under conditions of the OCM reaction. The low activity towards the isotopic exchange did not correlate with high activity in the OCM reaction. Therefore, their results do not support the heterolytic breaking of the C–H bond. Another test for the participation of basic sites in CH_4 activation is to analyze the influence of CO_2 on the activity and selectivity of the OCM reaction, since CO_2 is a poison for basic sites. Sinev et al. [44] measured the heat of CO_2 adsorption over PbO/Al_2O_3 and M_2O (M = Li, Na, K and Cs) on MgO; the lower the heat of adsorption, the lower is the basicity. The latter authors found an inverse correlation between the heats of adsorption and the rates of C_2 product formation, i.e. there is no evidence for the heterolytic nature of C–H bond breaking. Dissanayake et al. [43] studied the influence of CO_2 on the OCM reaction and simultaneously on the H–D exchange. They found that CO_2 strongly inhibited the exchange reaction but did not influence the activity of the OCM reaction. These results indicate the existence of two types of catalyst sites for methane activation; one is responsible for the H–D exchange and the other participates in the OCM reaction. Since CO_2 is always present under conditions of the OCM reaction, it is expected that basic sites, which are responsible for the heterolytic breaking of the C–H bond, will not contribute substantially to CH_4 activation. They may be active only at very low degrees of methane conversion.

Summarizing the above discussion, the formation of gas-phase methyl radicals is well proven. The homolytic mechanism of breaking the C–H bond in the methane molecule is more frequently accepted in the scientific community than the heterolytic mechanism.

Once formed, methyl radicals participate in several gas-phase or heterogeneous reactions leading to various reaction products. These reactions determine the selectivity of the OCM reaction. The recombination of two methyl radicals in the gas phase yields ethane [Eq. (4)]. Ethene is formed either via homogeneous or heterogeneous ethane dehydrogenation. According to repeatedly reported selectivity–conversion relationships of the OCM reaction (Fig. 1) over various catalytic materials, carbon oxides are formed from methane in addition to consecutive oxidation of C_2 products. The following discussion starts with the mechanistic analysis of the undesired CO_x formation from methane followed by that of consecutive transformations of ethane/ethene.

Besides their recombination [Eq. (4)], methyl radicals react with gas-phase O_2 forming $CH_3O_2^\bullet$ radicals [Eq. (5)], which were experimentally detected by ESR spectroscopy [45]. The $CH_3O_2^\bullet$ radicals are considered as precursors for CO_x formation [46, 47]. This conclusion is based on the fact that the equilibrium of reaction pathway (5) is shifted to $CH_3^\bullet$ and O_2 with an increase

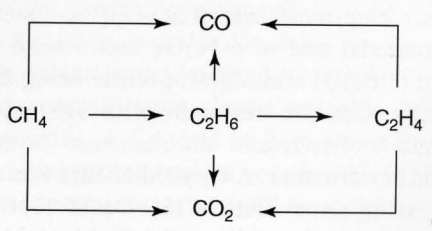

Fig. 1 Simplified scheme of the OCM reaction.

in temperature. Accordingly, the reaction temperature influences positively the selectivity towards C_2 products.

$$CH_3^\bullet + CH_3^\bullet \longrightarrow C_2H_6 \quad (4)$$

$$CH_3^\bullet + O_2 \rightleftharpoons CH_3O_2^\bullet \quad (5)$$

The formation of CO_x occurs also via pure heterogeneous transformations of $CH_3O_2^\bullet$, as suggested in Ref. [41]. Methyl radicals also undergo heterogeneous transformations. Lunsford and coworkers [48] studied the interaction of methyl radicals with oxides of rare earth metals. Methyl radicals were generated over Sm_2O_3 and passed over the studied oxides. The methyl radicals formed did not react with La_2O_3, Sm_2O_3, Nd_2O_3, Eu_2O_3 and Yb_2O_3 but reacted strongly with CeO_2, Pr_6O_{11} and Tb_4O_7. The last three catalysts are non-selective in the OCM reaction. Later, the same group determined sticking coefficients of $CH_3^\bullet$ radicals with various oxide catalysts [49]. They found that these coefficients are low over selective OCM catalysts but high over non-selective catalysts. Thus, methyl radicals can contact the surface of selective catalysts many times without any transformations before they recombine to give ethane. Anshits and coworkers [50] suggested that methoxy species are formed via reaction of methyl radicals with O^{2-}_{cus} (cus = coordinatively unsaturated sites) according to Eq. (6). These species are further transformed to CO [Eq. (7)]. This statement was made taking the CO:H_2 ratio into account, which was close to 2:3 [see Eq. (7)].

$$CH_3^\bullet + O^{2-} \longrightarrow CH_3O^{2-} \quad (6)$$

$$CH_3O^{2-} \longrightarrow CO + \frac{3}{2}H_2 \quad (7)$$

Consecutive oxidation of ethane to ethene and CO_x occurs via homogeneous and heterogeneous reaction steps, the latter playing the most significant role. As found in Ref. [51], methane inhibits homogeneous oxidation of ethene. The initial step of ethane activation is the breaking of a C–H bond in the molecule by a surface oxygen species. This reaction competes with methane activation [Eqs. (1) and (3)]. Due to the lower binding energy of the C–H bond in the C_2H_6 molecule than in CH_4, the rate of ethane activation is 5–20 times higher than that of methane activation [52, 53]. The ethyl radicals formed can be further dehydrogenated to ethene on the catalyst surface or react with gas-phase oxygen to give $C_2H_5O_2^\bullet$ radicals, which were detected experimentally [53, 54]. These radicals can undergo further reactions to ethene or CO_x products.

Summarizing the above discussion, ethane is a primary product of the recombination of two methyl radicals. The ethane formed undergoes further transformations to ethene and carbon oxides. Both hydrocarbons are consecutively oxidized to CO_x. Due to the higher reactivity of ethane and ethene as compared with methane, combustion of C_2 hydrocarbons becomes the main route of CO_x formation, when the degree of methane conversion increases. Accordingly, the contribution of direct methane oxidation to CO_x decreases. Selectivity towards selective and non-selective reaction pathways can be tuned by the catalyst composition and reaction engineering. The next two sections are focused on the role of reactive oxygen species and structural defects in the OCM reaction. Reaction engineering and modeling are thoroughly discussed in Section 13.17.3.

13.17.2.3 Oxygen Species in the OCM Reaction

It is well accepted that surface oxygen species are required for methane activation [Eqs. (1) and (3)]. However, there is no unanimous agreement on the nature of these reactive oxygen species. This is due to the variety of the OCM catalysts and due to the experimental limitations for unambiguous identification of active sites at high temperatures (>973 K) of the OCM reaction.

The importance of the nature of oxygen species is indirectly supported by the results of the OCM reaction, where different oxidizing agents were used [55–61]. Figure 2 clearly demonstrates an increase in C_2 selectivity when O_2 is replaced by N_2O. However, contradictory results were reported in [55]. For Na/CaO and Li/CaO catalytic materials with low (<2 at.%) Li and Na loading [56, 58, 59], the difference in catalytic performance on using O_2 or N_2O was related to the different oxygen species generated from O_2 and N_2O. Oxygen adsorption was suggested to

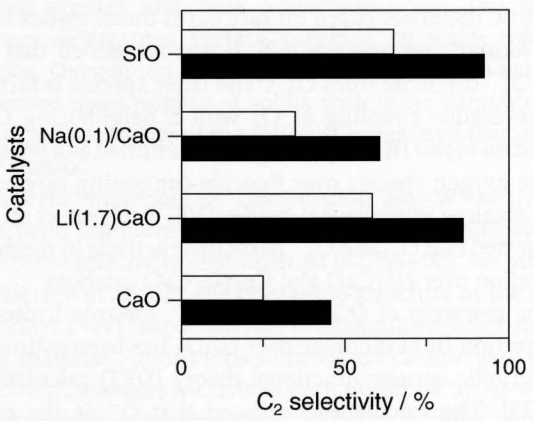

Fig. 2 C_2 selectivity ($C_2H_4 + C_2H_6$) over various catalytic materials. Conditions: T = 1023 K, CH_4:O_2:He = 30:15:55 (empty bars), CH_4:N_2O:He = 30:30:40 (solid bars), $X(CH_4)$ < 4%. The data are from Refs. [56, 62, 63].

References see page 3021

occur via a molecular precursor followed by its dissociation to O^{2-}_{cus} and non-charged atomic oxygen (O). The latter is selective and also generated upon N_2O activation. The O^{2-}_{cus} species was assumed to participate in CO formation [Eqs. (6) and (7)], since the rate of CO formation decreased strongly upon replacing of O_2 by N_2O.

Oxygen adsorption over OCM catalysts takes place on oxygen anion vacancies or on interstitial sites if the oxide structure enables oxygen to enter these sites [64]. This general mechanism is expected to be similar for oxides of reducible and non-reducible metals. However, the nature of oxygen species is different. Lattice oxygen (O^{2-}) is an active species on easily reducible metal oxides. It is formed directly from gas-phase oxygen. In this reaction, the metal cation changes its oxidation state followed by electron transfer to oxygen. Due to a significantly higher bandgap in oxides of non-reducible metals as compared with the reducible metals, differently charged oxygen species (O^-, O^-_2, O^{2-}_2, O^{2-}_3 and O^{2-}) can exist on the catalyst surface. Intrinsic (anion vacancies, interstitial sites) and impurity defects in these oxides play a significant role in electronic transfers, since the metal cations cannot change their oxidation state.

Sinev et al. [65] and Otsuka et al. [66] showed that Na_2O_2 and BaO_2 converted methane to ethane and CO_x. These results prove the ability of O^{2-}_2 species for methane activation. By means of *in situ* Raman analysis, O^{2-}_2 species were identified over Na/La_2O_3 and Sr/La_2O_3 at 973 K [67] and over BaO/MgO [68] at 973 and 1023 K. The latter authors found that these species reacted fast with CO_2 to form carbonates, i.e. no peroxide species were observed in the presence of CH_4 and O_2 above 970 K. In addition to O^{2-}_2, O^-_2 species were also observed over catalytic materials based on rare earth metal oxides by *in situ* Raman spectroscopy [69]. It was suggested that O^-_2 and O^{2-}_2 originate from O^{2-}_3. The latter species is formed via reversible coupling of O_2 with a neighboring O^{2-}. Based on *in situ* IR analysis, O^-_2 was identified as a possible active oxygen species over fluoride-containing rare earth and alkaline earth metal oxides [70]. Pacheco et al. [71] suggested that O^- and O^{2-}_2 participate actively in methane activation over Na/CaO and Ce/Na/CaO catalysts.

The reactivity of O^-, O^{2-}_2 and O^{2-} towards hydrogen abstraction from methane over La_2O_3 has been estimated by periodic density functional theory (DFT) calculations [72, 73]. The calculations showed that O^- is the most reactive oxygen species. Peroxide species have slightly lower activity for H abstraction. The authors suggested a reaction mechanism according to which O^{2-}_2 but not O^- participates in the breaking of a C–H bond in the methane molecule. However, they did not completely exclude the participation of O^-.

The importance of O^- oxygen species in the OCM reaction has been repeatedly highlighted by Lunsford and associates [36, 48]. These authors identified M(Li or Na)$^+O^-$ centers in Li/MgO, Li/ZnO and Na/CaO catalysts by means of ESR spectroscopy. Since the M^+O^- centers were identified in the bulk of the catalysts, these authors suggested that equilibrium exists between bulk and surface species.

Baerns and coworkers have comprehensively studied oxygen adsorption over rare earth and alkaline earth metal oxides by means of contact potential difference measurements [74, 75] and kinetic analysis [76–78]. In agreement with the above mechanistic concept of O_2 adsorption, they found that adsorbed molecular and atomic oxygen species are formed from O_2. The relative coverage of the catalyst surface by these oxygen species is influenced by the oxygen partial pressure: the higher the oxygen partial pressure, the higher is the concentration of adsorbed molecular oxygen species. Doping of Nd_2O_3 with SrO and CaO with Na_2O accelerates the transformation of molecular to atomic adsorbed oxygen species. This phenomenon was related to the creation of anion vacancies in the oxide lattice on adding low-valency additives into the host oxide matrix. Anion vacancies are important for O_2 adsorption and further dissociation of molecular to atomic adsorbed oxygen species [74, 76]. The selectivity of C_2 products over Na_2O/CaO catalysts was found to depend on the Θ_O/Θ_{O_2} ratio (Θ_O and Θ_{O_2} are surface coverages by atomic and molecular adsorbed oxygen species, respectively). The ratios were estimated at the same oxygen partial pressures as in the catalytic runs. From Fig. 3, it is clearly seen that the higher the Θ_O/Θ_{O_2} ratio, the higher is the selectivity. The increase in the C_2 products selectivity with decreasing concentration of adsorbed molecular oxygen species can be due to the fact that the oxygen species consisting of more than one oxygen atom promote especially C–C bond cleavage [79]. This reaction is probably the initial step of the combustion of C_2 products. The positive effect of the transformation of molecular oxygen in atomic oxygen surface species on OCM selectivity has been reported [78, 80].

13.17.2.4 Structural Defects and Related Physicochemical Properties

Voskresenskaya et al. [64] thoroughly reviewed the literature on the role of structural defects for oxidant activation in the OCM reaction up to 1994. The importance of the structural defects was confirmed in recent work [19, 74, 76, 80–85]. Voskresenskaya et al. divided all known OCM catalysts into two groups: (i) multiphase catalysts and (ii) single phase catalysts [64]. The main defects and oxygen species in these two catalyst groups are shown in Table 2. Structural defects influence the type of electrical

Tab. 2 Systematization of OCM catalysts. Reproduced from Ref. [87]

Catalyst type	*Active oxygen sites*	*Type of defects*
I. Multi-phase catalysts (high content of promoters)	(a) Surface promoter compound	
	(b) Compound of promoter with oxide matrix	
II. Single-phase catalysts		
Individual compounds:		
(i) Rare earth oxides (except Pr, Ce, Tb oxides)	O_2^{2-} and/or O_2^-	Oxygen vacancies at $p < 0.1$ kPa
		Interstitial (O_i) or active oxygen species at $p > 0.1$ kPa
(ii) Alkaline earth oxides	O_2^{2-}, O^-, O_{cus}^{2-} and O^0 (uncharged)	
Solid solutions based on alkaline earth oxides	O_2^{2-}, O^-, O_{cus}^{2-} and O^0 (uncharged)	Oxygen vacancies at p < 0.1 kPa
		active oxygen species at p > 0.1 kPa
		Impurity defects (transition metals)

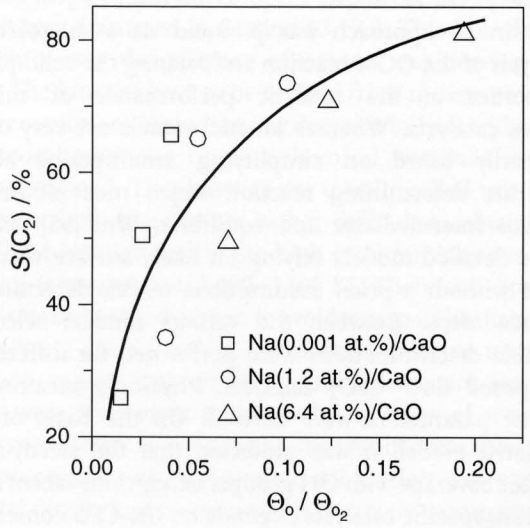

Fig. 3 Selectivity of C_2 products over Na_2O/CaO catalysts versus steady-state Θ_O/Θ_{O_2} ratio simulated at oxygen partial pressures without the presence of methane. Reproduced from Ref. [75].

conductivity of solid materials. The electrical properties play an essential role in the OCM reaction [86]. Solid materials of n-type conductivity are usually non-selective catalysts. It appears that solids containing both p-type and oxygen-ion conductivity are desirable catalysts [74, 76, 80]. It must be stressed that the bandgap should be in the range 5–6 eV.

The necessity for p- and ionic-type conductivities can be understood from the following discussion. As mentioned in Section 13.17.2.3, differently charged adsorbed oxygen species are considered to be responsible for methane activation. To form charged oxygen species, electrons from the solid should be transferred to oxygen. It is well known that the concentration of electrons in the conduction band is a function of the bandgap: the lower the bandgap, the higher is the concentration of electrons. Therefore, if the bandgap is too small, high concentrations of active oxygen species are expected, which do not favor selective methane oxidation. If the bandgap is too high, reactive oxygen species can hardly be formed and no catalytic activity is observed. It may be expected that an optimized concentration of active oxygen species is required for selective catalyst performance. This may be one reason why all selective OCM catalysts possess a bandgap of 5–6 eV. The oxygen ionic conductivity promotes both dissociation of adsorbed molecular oxygen species, which favor the consecutive oxidation of C_2 hydrocarbons, and fast exchange between surface atomic oxygen species and bulk anion vacancies. The latter process determines surface coverage by active oxygen species. Oxygen-ion and p-type conductivities are usually increased upon doping of solids with other compounds, if the oxidation state of the cation is lower than that in the host matrix.

Catalytic materials of composition $Na-W-Mn/SiO_2$ have been intensively characterized in order to establish structure–selectivity relationships [82, 88–90]. According to Palermo et al. [82], the crystalline structure of the support plays a very important role in designing a selective catalytic material. Amorphous silica led to a catalyst with poor selectivity, whereas α-cristobalite (crystalline SiO_2) was a very favorable supporting material. The authors pointed out that Na plays a dual role: (i) crystallization of amorphous silica to the crystalline form and (ii) stabilization and dispersion of surface WO_x species. WO_4 was mentioned as a possible candidate. The importance of WO_4

References see page 3021

species was later highlighted by Green and coworkers [88–90], who catalytically tested and characterized a series of Na–W–Mn/SiO_2 catalytic materials by means of XPS, Raman spectroscopy and XRD analysis. DFT calculations by Chen et al. [91] predicted that the tetrahedral [WO_4] site with a single bridge oxygen is the most probable active center responsible for methane activation.

Anshits and coworkers [56, 58, 59, 62, 92] demonstrated that the defect structure of OCM catalysts is strongly changed under reaction conditions. They used the following methodology. A sample was treated in a reactive feed (O_2, N_2O, He, CH_4–O_2 or CH_4–N_2O) at 1023 K followed by rapid quenching of the pretreated sample from 1023 to 77 K. The quenched samples were γ-irradiated. The irradiation did not create new defects but made them visible by EPR spectroscopy. These structural changes influence the catalytic performance. For Li/CaO and Na/CaO with low (<2 at.%) promoter (Li or Na) content, [M(Li or Na)CO_3]$^-$, CO_2^{2-} and O_3^{2-} defects were identified in the volume of the CaO lattice after the OCM reaction with O_2 took place at 1023 K. A correlation between the type of defects formed and C_2 selectivity was established [92]. An increase in the fraction of the [M(Li or Na)CO_3]$^-$ centers in doped CaO resulted in a rise in C_2 selectivity using an O_2-containing reaction feed. CO_2^{2-} species were considered as precursors for CO, and O_3^{2-} was assumed to be a non-selective oxygen species. On using N_2O as oxidant, no visible changes in the catalyst volume were observed. The differences in catalytic performance were related to the nature of the oxygen species generated from O_2 and N_2O.

The importance of reaction-induced changes in the silver-catalyzed OCM reaction was demonstrated by Nagy et al. [93]. The structural changes were claimed to be responsible for an increase in C_2 selectivity with time-on-stream. The silver surface underwent strong morphological changes under reaction conditions. The poor initial selectivity was ascribed to the reaction of methane with O_α (chemisorbed, surface-bound atomic oxygen) surface species. Its concentration was assumed to be high due to the high ability of polycrystalline silver to produce these species. The rough silver surface becomes faceted with time-on-stream. The faceting promotes the formation of O_γ species (nucleophilic species embedded in the uppermost layer of silver atoms), which were suggested to be responsible for improved catalytic performance.

13.17.2.5 New Approaches in Catalyst Design

The past development of new OCM catalysts was mainly based on empirical approaches applying the knowledge that had been accumulated during the past. The most important catalyst properties have been thoroughly discussed in Sections 13.17.2.2–13.17.2.4. All the numerous studies led to maximal C_2 selectivities (ethene + ethane) in the order of 70–85% at degrees of methane conversion from 30 to 40%. Due to the limited degree of methane conversion achievable, C_2 yields of only 20–30% were generally obtained in a one-pass reactor operation (see Table 1).

Ying and colleagues [94] reported, on the basis of assumed fundamental kinetics, an upper limit in C_2 yield for non-porous catalysts not exceeding 28%. The basic idea behind their approach was to identify selectivity- and activity-determining elementary surface and also gas-phase reaction steps. By varying their kinetic parameters within reasonable boundaries, their influence on selective and non-selective reaction pathways was assessed. The challenge of future work in catalyst development for OCM will be the design of specific functions of catalytic materials that favor C_2 selectivity and suppress non-selective reaction steps.

A similar approach was pursued via a microkinetic analysis of the OCM reaction and relating the solid-phase properties to the catalytic performance of mixed-oxides catalysts. Whereas kinetic models are very often primarily based on simplifying assumptions about the rate determining reaction steps, most abundant surface intermediates and equilibria, Wolf [95] set up more detailed models relying on likely surface reaction steps without *a priori* assumptions of rate-determining surface steps. Between the various models selected, suitable discriminations were performed for differently composed CaO–CeO_2 catalysts. Physically meaningful kinetic parameters were derived. On the basis of the validated model, it was predicted that the steady-state surface coverage with OH groups, oxygen and vacant sites of these specific catalysts depends on the CaO content of the mixed metal oxides. Subsequently, the same group predicted relationships for the same catalysts between their catalytic and solid-phase properties [96]. The surface of solid solutions of CaO in CeO_2 was characterized by XPS, UPS, ISS and IR methods. Changes in surface properties could be related to the electrical conductivity of the materials. The oxygen anion conductivity increases and a change from n- to p-type conductivity occurs with increasing CaO content. Without going into details, it was shown that ethane plus ethene selectivity depends on methyl radical formation and concentration. Both of these reaction pathways are affected by methane dissociation which takes place on stable surface OH groups, which, in turn, are related to catalyst composition and the resulting surface properties. Strong indications can be derived for catalyst improvement on the basis of the microkinetic analysis. This is in agreement with some of the findings put forward in the preceding sections.

One promising way of pursuing catalyst development on the basis of knowledge as pointed out above would be the application of combinatorial computational catalytic chemistry as outlined elsewhere [97] combined with high-throughput experimentation. Huang et al. [98] reported an interesting attempt that comes close to this by using an artificial neural network and a hybrid genetic algorithm. Basic and acidic and also redox-type materials were incorporated in the catalyst composition, leading to a maximum C_2 yield of 27.8% ($S = 73.5\%$, $X_{C_2} = 37.8\%$), which, within experimental error, is equal to the "kinetic" value reported above by Ying and coworkers [94].

13.17.3 Reaction and Process Engineering

The basis of reaction engineering modeling and simulation is the knowledge of reaction kinetics describing the various steps within the complex OCM reaction network, which was discussed in Section 13.17.2. This knowledge usually serves the purpose of process engineering design. The kinetics have to be derived from measurements under conditions excluding any disguise by heat and mass transport limitations, i.e. pure chemical processes have to be investigated. This kinetics are usually called intrinsic kinetics. Such kinetics are rather difficult to obtain for the OCM reaction due to the high exothermicity and operating temperatures (1000–1300 K). Therefore, special precautions have to be taken to avoid transport limitations.

Applying such kinetics and suitable reactor models, reaction engineering modeling and subsequent simulations were frequently reported. Many types of reactors were considered; in most cases, the results were validated by appropriate experimentation. All models and experimental results had in common incomplete conversion of methane due to a high stoichiometric excess of methane with respect to oxygen; thereby the formation of side products, CO and CO_2, was partly suppressed. Traces of acetylene and C_{3+} hydrocarbons were generally not considered in modeling. It is obvious that significant separation efforts are required to isolate all the ethene from the side products.

In the following sections, kinetics of the OCM reaction and the performance, modeling and simulation of reactor operation are dealt with. Innovative process engineering aspects for facilitating separation are indicated.

13.17.3.1 Chemical Kinetics

Early work on the kinetic analysis of the OCM reaction over Na/MgO [99] and Na/CaO [100] catalysts was based on hyperbolic Hougen–Watson-type and power-law rate equations. Mechanistic conclusions were derived in both studies. A surface science approach in setting up kinetic models and determining their kinetic parameters was already outlined above in Section 13.17.2.5.

The most comprehensive intrinsic kinetics up to date, which consist of three primary and seven consecutive pseudo-elementary reaction steps, was reported in 1997 by Stansch et al. [101]. The kinetics are based on an La_2O_3/CaO-catalysed OCM reaction network as presented in Fig. 4. This mechanistic scheme considers the formation of ethane and ethene and also of CO and CO_2 via different reaction routes, including one gas-phase reaction step. The estimated frequency factors and apparent activation energies for the various reaction steps and adsorption enthalpies for some compounds were also reported. Tye et al. [102] later confirmed the suitability of Stansch et al.'s kinetic model within the context of isothermal and adiabatic fixed-bed reactor modeling for the same catalyst.

13.17.3.2 Modeling, Simulation and Performance of Catalytic Reactors

Most of the initial experimental work in OCM was done in laboratory-scale catalytic fixed-bed reactors. The experiments and simulation studies showed that axial and radial temperature gradients existed in the reactors due to the high exothermicity of the reaction. These gradients had to be avoided by appropriate measures (e.g. dilution of the catalytic bed with inert materials and sufficient cooling of small-diameter test reactors by immersing them in fluidized beds). Thereby, disguise of the performance and the kinetics of the catalysts could be mostly eliminated.

Conventional catalytic fixed-bed reactors are not the issue in this chapter since sufficient attention has been paid to them in the past [103]. Instead, plug-flow reactors with distributed oxygen addition, counter-current moving-bed chromatographic reactors, fluidized-bed reactors and various types of membrane reactors are dealt with.

13.17.3.2.1 Distributed Oxygen Supply to a Catalytic Fixed-Bed Reactor Androulakis and Reyes [104] modeled and simulated a staged catalytic fixed-bed reactor with

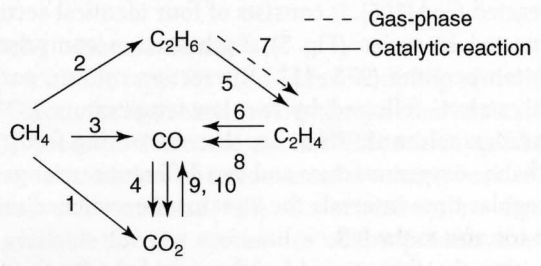

Fig. 4 Reaction scheme and pathways from Ref. [101].

References see page 3021

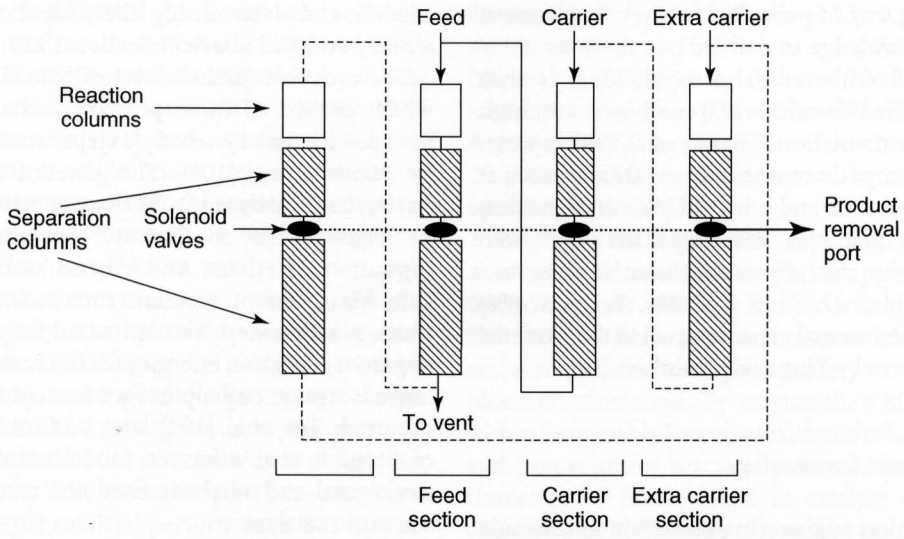

Fig. 5 Schematic overview of the counter-current moving-bed chromatographic reactor. (There is no flow through the dashed lines. The inlet ports move during operation to the left.) Reprinted from Ref. [106].

distributed and co-fed oxygen addition and product removal over 20 stages. The model includes homogeneous and heterogeneous reactions. By a rigorous optimization algorithm, C_2 yield was maximized up to 87% over the 20 stages. This maximum is, however, surprisingly independent of the form in which oxygen is added, i.e. co-fed or staged. The work systematically explored the use of controlled oxygen addition and product removal schemes that improve the performance of the OCM reaction. The essential of the approach is the removal of C_2 products between stages, thereby preventing their further total oxidation. This represents a significant progress over the earlier suggestion of applying distributed oxygen addition alone, i.e. without inter-stage separation of hydrocarbon products [105].

13.17.3.2.2 **Counter-Current Moving-Bed Reactor** The counter-current moving-bed chromatographic reactor serves the purpose of carrying out the OCM reaction and simultaneously separating the C_2 hydrocarbons from the unreacted feed [106]. It consists of four identical sections connected in series (Fig. 5). Each section comprises a high-temperature (973–1123 K) reaction column packed with catalyst, followed by two low-temperature (373 K) separation columns. There are three incoming feeds: the methane–oxygen mixture and two different carrier gases. At regular time intervals the streams are switched to the next column to the left.

During the first period, methane is fed into the feed section amounting to about 15% of the carrier gas; oxygen is fed in such a way that methane-to-oxygen ratio amounts to 30:1. The feed is swept along by the carrier gas, which is introduced in the preceding column. The effluent from the reaction column is introduced to the separation section. The time interval between switching is determined such that the flows are switched just before the methane breaks through the second adsorption column in the feed section. The strongly retained products are held up in the first separation column. Immediately after the first switch, the carrier stream replaces the feed stream. It carries the unreacted methane to the new feed section. The feed stream now becomes a make-up feed, replacing the methane, which was reacted or was lost in the previous section, in addition to all necessary oxygen needed to maintain the methane-to-oxygen ratio. At the end of the second switching period, the products start to break through the first separation column. They are removed with the use of a second (extra) carrier during the next switching period, two sections behind the feed. All successive switching times are identical after the first one.

A C_2 yield of 55% at a methane conversion of 75% was achieved over a $YBa_2Zr_3O_{9.5}$ catalyst under optimal operating conditions. This yield exceeds one-pass catalytic fixed-bed operation using a co-feed of methane and oxygen. However, it appears highly unlikely that such a process, which is very interesting from a scientific point of view, can become economically viable due to the requirement for recycling huge amounts of unconverted methane.

13.17.3.2.3 **Fluidized-Bed Reactors** As outlined above, heat management for the highly exothermic OCM reaction is essential for reactor operation. Fluidized beds are very much suited for efficient heat removal.

Isothermal operation was achieved even at high per-pass conversions of methane when applying undiluted feeds (see, e.g., [107, 108]). Comparable or even higher C_2 yields were achieved in fluidized-bed than fixed-bed reactors. Pannek and Mleczko [109] modeled a fluidized-bed reactor using the so-called bubble-assemblage model of Kato and Wen [110] and the kinetics of Stansch et al. [101] for an La_2O_3/CaO catalyst (Fig. 4) and also the kinetics for homogeneous gas-phase reactions [111]. The performance of two laboratory-scale reactors (i.d. 5 and 7 cm) could be predicted within 20% accuracy. Similar results were obtained by Pugsley and Berruti [112], who extended their modeling to fluidized beds with internal circulation. Later, Pannek and Mleczko showed for an industrial fluidized-bed reactor that lower mass transfer coefficients result in larger contact times in the bubble phase, leading to total oxidation as compared with a laboratory-scale fluidized bed. This result underlines the importance of consecutive reactions and gas-phase reactions, which are promoted by the hydrodynamics of a large fluidized bed. For more accurate predictions of laboratory-scale reactors, homogeneous gas-phase reactions should not be neglected [113].

13.17.3.2.4 **Membrane Reactors** High concentrations of oxygen are detrimental to high C_2 selectivities. Low oxygen concentrations are, however, unfavorable for high degrees of methane conversion and high C_2 yields. This led to the concept of distributed oxygen delivery along the reactor length, as already described above (see Section 13.17.3.2.1). An alterative to staged oxygen delivery is the use of membrane reactors, which started to be applied in OCM in the late 1980s/early 1990s (see, e.g., Refs. [114–117]). An early overview of previous work was given by Eng and Stoukides for catalytic and electrocatalytic OCM with solid oxide membranes [118].

Membrane reactors used in OCM can be divided into three groups based on the principles of oxygen permeability: (i) gas-phase oxygen simply diffuses through a porous membrane (e.g. γ-Al_2O_3); (ii) oxygen is transported as O^{2-} species through an oxygen-ion conducting membrane; (iii) oxygen is electrocatalytically transported as O^{2-} from the cathode surface through a solid electrolyte to the anode. Figure 6 illustrates schematically the above membrane reactors and a fixed-bed reactor (FBR) with plug-flow.

Kao et al. [119] simulated OCM performances of a co-fed FBR and a ceramic dense-membrane reactor (DMR) (Fig. 6c) made of a mixed-conducting material. Both reactors were packed with Li/MgO catalyst. The concentration of the oxygen transported through the membrane was lower within the DMR than in the FBR. The performance of the DMR led to a significantly increased C_2 selectivity and yield as compared with the FBR. Such mixed-conducting ceramic membranes ($La_{0.8}Sr_{0.2}Co_{0.6}Fe_{0.4}O_{3-\delta}$) were prepared via different synthesis approaches by the same group [120]. The oxygen fluxes through a 1.85-mm thick membrane amounted to ca 10^{-9}–10^{-7} mol cm^{-2} s^{-1}. The experimental results are not in full agreement with the simulations, i.e. experimental selectivities and yields were lower than predicted by Kao et al. [119]. They could be only maintained when the catalytic surface properties of the membrane were not impaired by low oxygen partial pressures. In a subsequent paper [121], it was reported that bulk diffusion of electron holes is the rate-limiting step for oxygen permeation. As predicted by the above-mentioned simulations, it was shown experimentally that higher selectivities could be achieved by the membrane reactor than in the FBR. These partly different results indicate that the type and composition of the membranes influence the catalytic performance of a membrane reactor. Hence it is not surprising that various studies were concerned with the preparation and testing of different membranes. None of them reached single-pass methane conversions of 35–37% and C_2 selectivities of 85–88%, which is equivalent to yields of 30% as required for achieving commercial feasibility [122].

In a most recent comparative study of different kinds of reactors for the OCM reaction, Kiatkittipong et al. [123] found that FBR is not recommendable for OCM, whereas porous membrane reactors (PMR) (Fig. 6b) and mixed ionic and electronic conducting membrane reactors (MIEMR) (Fig. 6c) were suitable at temperatures around 1150 K. However, the use of PMR is not recommended in the case of air feed or oxygen feed containing impurities. Operation at high pressure was beneficial only for MIEMR and SOFCR (solid oxide fuel cell reactor) (Fig. 6d). The drawback of PMR was the methane loss through the non-selective porous membrane and that of SOFCR was the requirement for approximately 200 K higher operating temperatures compared with the others; the electricity generated as a by-product might make SOFCR still attractive.

13.17.3.3 **Process Concepts**

All process concepts for the oxidative coupling of methane suffer from the high costs for low-temperature separations of C_2 products from the reactor effluent containing a high concentration of unconverted methane besides the various side products [124]. Unfortunately, no figures are available for the economics of the process concept based on the counter-current moving-bed reactor (see Section 13.17.3.2). A new concept consisting of thermal

References see page 3021

line amortization, 25% fixed costs and US$1–3 per barrel operating costs.

As claimed in [126], the economy of methane-to-ethene processing can be improved when both the catalytic OCM reaction and the separation of ethene from the reactor-effluent components (methane, ethane, carbon oxides) are performed at elevated pressure. Elevated pressures reduce not only the size of the various process units due to an increase of the reaction rates but they improve also the efficiency of the separation process. For separating the ethene an aqueous silver-nitrate solution was used as a complexing absorbent.

13.17.4 Conclusion

Fundamental understanding of the complex heterogeneous–homogeneous reaction network of the OCM reaction has progressed significantly since its infancy in the early 1980s. Many selectivity- and activity-determining factors have been identified. Selective catalytic materials should generate methyl radicals without their consecutive heterogeneous oxidation. The most challenging property of the selective catalytic materials is their ability to activate methane in the presence of more reactive reaction products (C_2H_4 and C_2H_6), which are the essential CO_x precursors. The above catalyst properties can be partially tuned by appropriate catalyst design taking into account the knowledge from surface science and related kinetic studies. Despite a good knowledge of the fundamentals of the OCM reaction, per-pass yields of C_2 hydrocarbons higher than 30% under conditions close to the anticipated practice have not been achieved. It is not expected that higher values will be achieved in the near future based on present catalyst design only. Catalytic reaction engineering design appears to be helpful for further improvement of the OCM performance. For the reactor design, i.e. fixed-bed, fluidized-bed, countercurrent moving bed and membrane reactors, modeling, simulation and operation, significant knowledge and basic understanding have been accumulated. All process designs, however, suffer from the high costs of separation of the products from unconverted methane and the required gas recycling. As soon as this challenge has been successfully met, the conversion of methane will certainly become economically viable.

References

1. P. F. van den Oosterkamp, in *Encyclopedia of Catalysis*, I. Horvath (Ed.), Vol. 6, Wiley-VCH, Weinheim, 2003, p. 770.
2. *Ullmann's Encyclopedia of Industrial Chemistry, Vol. 10, Cyano Compounds, Inorganic*, Wiley-VCH, Weinheim, 2003, p. 774.
3. G. F. Keller, M. M. Bhasin, *J. Catal.* **1982**, *73*, 9.
4. W. Hinsen, M. Baerns, *Chem. Z.* **1983**, *107*, 223.
5. T. Ito, J. H. Lunsford, *Nature* **1985**, *314*, 712.
6. (a) E. E. Wolf (Ed.), *Methane Conversion by Oxidative Process. Fundamentals and Engineering Aspects*, Van Norstrand Reinhold, New York, 1992 548 p. (b) M. Baerns p. 382–402 in 6(a).
7. V. D. Sokolovskii, E. A. Mamedov, *Catal. Today* **1992**, *14*, 415.
8. M. Baerns, J. R. H. Ross, in *Perspectives in Catalysis*, J. M. Thomas, K. I. Zamaraev (Eds.), Blackwell, Oxford, 1992, p. 492.
9. J. H. Lunsford, *Catal. Today* **1990**, *6*, 235.
10. *Ullmann's Encyclopedia of Industrial Chemistry, Vol. 1, Acetylene*, Wiley-VCH, Weinheim, 2003, p. 785.
11. J. S. Lee, S. T. Oyama, *Catal. Rev. Sci. Eng.* **1988**, *30*, 249.
12. O. V. Krylov, *Catal. Today* **1993**, *18*, 209.
13. A. C. Jones, J. J. Leonardo, A. J. Sofranko, US Patent 4 443 644, assigned to Atlantic Richfield, 1984.
14. A. M. Gaffney, C. A. Jones, J. J. Leonard, J. A. Sofranko, *J. Catal.* **1988**, *114*, 422.
15. E. V. Bezrukov, E. S. Bobkova, L. N. Kurina, V. N. Belousova, *Pet. Chem.* **2004**, *44*, 261.
16. A. I. Bostan, Y. I. Pyatnitskii, L. N. Raevskaya, V. G. Pryanikova, S. A. Nedil'ko, A. G. Dzyaz'ko, E. G. Zen'kovich, *Theor. Exp. Chem.* **2005**, *41*, 32.
17. T. Ito, J. Wang, C.-H. Lin, J. H. Lunsford, *J. Am. Chem. Soc.* **1985**, *107*, 5062.
18. C. T. Au, K. D. Chen, C. F. Ng, *Appl. Catal. A* **1998**, *170*, 81.
19. C. T. Au, X. P. Zhou, Y. W. Liu, W. J. Ji, C. F. Ng, *J. Catal.* **1998**, *174*, 153.
20. V. R. Choudhary, V. H. Rane, S. T. Chaudhari, *Fuel* **2000**, *79*, 1487.
21. A. Palermo, J. P. H. Vazquez, R. M. Lambert, *Catal. Lett.* **2000**, *68*, 191.
22. Y. Zeng, F. T. Akin, Y. S. Lin, *Appl. Catal. A* **2001**, *213*, 33.
23. A. G. Dedov, A. S. Loktev, I. I. Moiseev, A. Aboukais, J. F. Lamonier, I. N. Filimonov, *Appl. Catal. A* **2003**, *245*, 209.
24. E. V. Fomenko, E. V. Kondratenko, O. M. Sharonova, V. P. Plekhanov, S. V. Koshcheev, A. I. Boronin, A. N. Salanov, O. A. Bajukov, A. G. Anshits, *Catal. Today* **1998**, *42*, 273.
25. E. V. Fomenko, E. V. Kondratenko, A. N. Salanov, O. A. Bajukov, A. A. Talyshev, N. G. Maksimov, V. A. Nizov, A. G. Anshits, *Catal. Today* **1998**, *42*, 267.
26. A. G. Anshits, E. V. Kondratenko, E. V. Fomenko, A. M. Kovalev, O. A. Bajukov, N. N. Anshits, E. V. Sokol, D. I. Kochubey, A. I. Boronin, A. N. Salanov, S. V. Koshcheev, *J. Mol. Catal.* **2000**, *158*, 209.
27. K. Otsuka, Q. Liu, M. Hatano, A. Morikawa, *Chem. Lett.* **1986**, 903.
28. A. N. Shigapov, M. A. Novozhilova, S. N. Vereshchagin, A. G. Anshits, V. D. Sokolovskii, *React. Kinet. Catal. Lett.* **1988**, *37*, 397.
29. R. Burch, G. D. Squire, S. C. Tsong, *Appl. Catal.* **1988**, *43*, 109.
30. B. Wharren, *Catal. Today* **1992**, *13*, 311.
31. J. H. Hong, K. J. Yoon, *Appl. Catal. A* **2001**, *205*, 253.
32. H. Abbas, H. Azzis, E. Bagherzadeh, Patent WO 2005 005042, assigned to HRD (USA) and National Petrochemical (Iran), 2005.
33. K. Machida, M. Enyo, *J. Chem. Soc., Chem. Commun.* **1987**, 1639.
34. M. Stoukides, *Catal. Rev.* **2000**, *42*, 1.

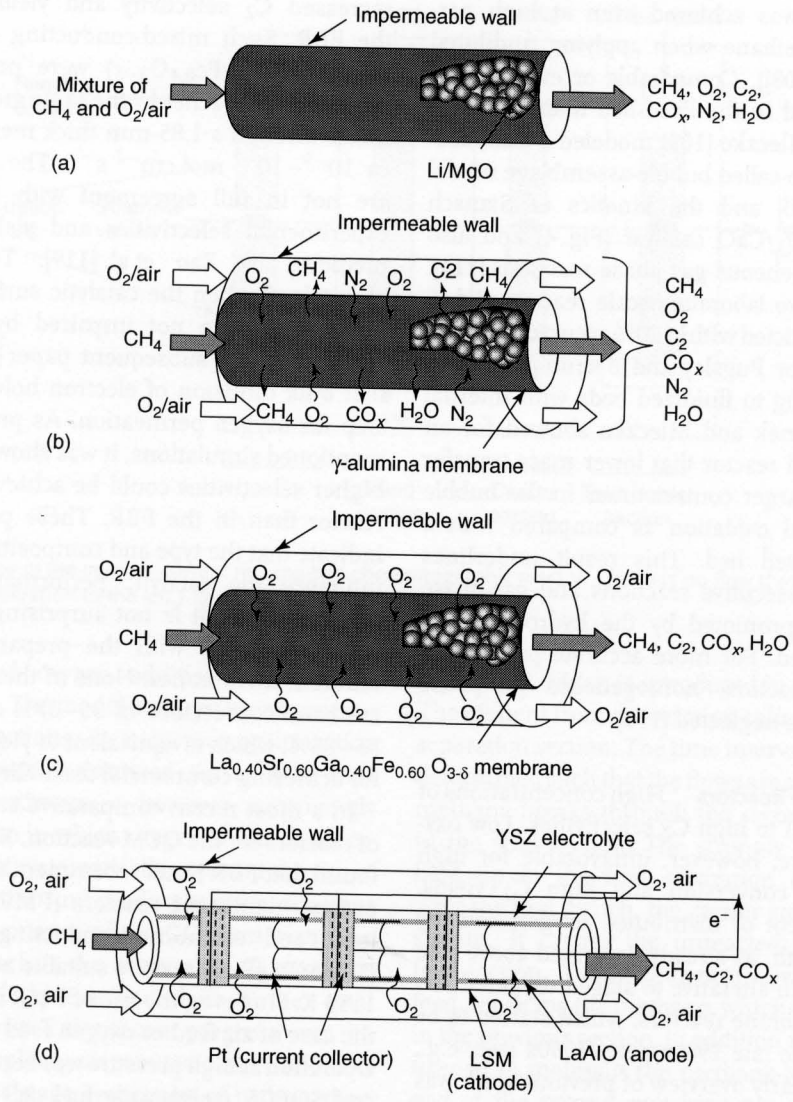

Fig. 6 Schematic overview of (a) fixed bed, (b) porous membrane reactor (PMR), (c) mixed ionic and electronic conducting membrane reactor (MIEMR) and (d) solid oxide fuel cell reactor (SOFCR). Reproduced from Ref. [123].

coupling of methane is mentioned below for the sake of completeness, namely the gas-to-ethene and gas-to-liquid process concept.

A process concept for converting natural gas into ethene and hydrogen or hydrocarbon liquids has been described more recently by Hall [125], being licensed by SynFuels International. This technology, which has been explored in an industrial pilot plant, is claimed to be economically viable depending on the methane price entering the overall cost scheme; thus, it can be considered attractive for remote gas or in situations where the gas is just flared off.

A portion of the methane feed (less than 10%) fuels an internal-combustion thermal cracker into which the remainder of the gas flows for cracking to mainly acetylene and hydrogen. Simultaneous coke formation is reduced by steam. The acetylene can then be hydrogenated with very high selectivity to ethene using the hydrogen from the cracker. For isolating the ethane, the stream is led into a separation unit, splitting out the ethene and hydrogen if desired. The remaining compounds would consist of methane, carbon monoxide, possibly hydrogen and nitrogen and its compounds (e.g. NO_x); the latter are removed and the remainder flows back to the cracker as fuel.

In principle, the process can be also directed towards liquid hydrocarbons by ethene oligomerization; in this way, it might substitute Fischer–Tropsch synthesis. The author reported some economic figures. For a 1.4 MSCMD (million standard cubic meters per day) plant US$25 per barrel of liquid product has been estimated assuming remote gas at US$0.018 m^{-3}, 10-year straight

35. S. Liu, X. Tan, K. Li, R. Hughes, *Catal. Rev.* **2001**, *43*, 147.
36. D. J. Driscoll, W. Martir, J.-X. Wang, J. H. Lunsford, *J. Am. Chem. Soc.* **1985**, *107*, 58.
37. J. H. Lunsford, P. G. Hinson, M. P. Rosynek, C. Shi, M. Xu, X. Yang, *J. Catal.* **1994**, *146*, 301.
38. O. V. Buyevskaya, M. Rothaemel, H. W. Zanthoff, M. Baerns, *J. Catal.* **1994**, *146*, 346.
39. O. V. Buyevskaya, A. I. Suleimanov, S. M. Aliev, V. D. Sokolovskii, *React. Kinet. Catal. Lett.* **1988**, *22*, 223.
40. V. D. Sokolovskii, G. M. Aliev, O. V. Buyevskaya, A. A. Davydov, *Catal. Today* **1988**, *4*, 293.
41. P. F. Nelson, C. A. Lukey, N. W. Cant, *J. Phys. Chem.* **1988**, *92*, 6176.
42. J. A. Lapszewicz, X.-Z. Jiand, *Catal. Lett.* **1992**, *13*, 130.
43. D. Dissanayake, J. H. Lunsford, M. P. Rosynek, *J. Catal.* **1994**, *146*, 613.
44. M. Y. Sinev, D. G. Filkova, V. Y. Bychkov, A. A. Ukharsky, O. V. Krylov, *Kinet. Katal.* **1991**, *32*, 157.
45. C. A. Jones, J. J. Leonard, J. A. Sofranko, *J. Catal.* **1987**, *103*, 311.
46. C.-H. Lin, K. D. Campbell, J.-X. Wand, J. H. Lunsford, *J. Phys. Chem.* **1986**, *90*, 534.
47. M. Y. Sinev, N. V. Korchak, O. V. Krylov, *Kinet. Katal.* **1987**, *28*, 1376.
48. Y. Tong, M. P. Rosynek, J. H. Lunsford, *J. Phys. Chem.* **1989**, *93*, 2386.
49. Y. Tong, J. H. Lunsford, *J. Am. Chem. Soc.* **1991**, *113*, 4741.
50. A. G. Anshits, N. P. Kirik, V. G. Roguleva, A. N. Shigapov, G. E. Setyutin, *Catal. Today* **1989**, *4*, 399.
51. S. Pak, P. Qiu, J. H. Lunsford, *J. Catal.* **1998**, *179*, 222.
52. M. Y. Sinev, V. N. Korchak, O. V. Krylov, *Kinet. Katal.* **1989**, *30*, 860.
53. E. M. Kennedy, N. W. Cant, *Appl. Catal.* **1991**, *75*, 32.
54. E. Morales, J. H. Lunsford, *J. Catal.* **1989**, *118*, 255.
55. G. J. Hutchings, J. R. Woodhouse, M. S. Scurrell, *J. Chem. Soc., Faraday Trans.* **1989**, *85*, 2507.
56. V. G. Roguleva, E. V. Kondratenko, N. G. Maksimov, G. E. Selyutin, A. G. Anshits, *Catal. Lett.* **1992**, *16*, 165.
57. H. Y. Yamamoto, H. Y. Chu, M. Xu, C. Shi, J. Lunsford, *J. Catal.* **1993**, *142*, 325.
58. A. G. Anshits, V. G. Roguleva, E. V. Kondratenko, *Studies in Surface Science and Catalysis*, Vol. 82, Elsevier, Amsterdam, 1994, p. 337.
59. E. V. Kondratenko, N. G. Maksimov, G. E. Selyutin, A. G. Anshits, *Catal. Today* **1995**, *24*, 273.
60. A. G. Anshits, E. V. Kondratenko, E. N. Voskresenskaya, L. I. Kurteeva, N. I. Pavlenko, *Catal. Today* **1998**, *46*, 211.
61. M. Bajus, M. H. Back, *Studies in Surface Science and Catalysis*, Vol. 119, Elsevier, Amsterdam, 1998, p. 289.
62. N. G. Maksimov, G. E. Selyutin, A. G. Anshits, E. V. Kondratenko, V. G. Roguleva, *Catal. Today* **1998**, *42*, 279.
63. V. G. Roguleva, M. A. Nikiphorova, N. G. Maksimov, A. G. Anshits, *Catal. Today* **1992**, *13*, 219.
64. E. N. Voskresenskaya, V. G. Roguleva, A. G. Anshits, *Catal. Rev. Sci. Eng.* **1995**, *37*, 101.
65. M. Y. Sinev, N. V. Korchak, O. V. Krylov, *Kinet. Katal.* **1986**, *27*, 1274.
66. K. Otsuka, Y. Murakami, Y. Wada, A. A. Said, A. Morikawa, *J. Catal.* **1990**, *121*, 122.
67. G. Mestl, H. Knözinger, J. H. Lunsford, *Ber. Bunsges. Phys. Chem.* **1993**, *97*, 319.
68. J. H. Lunsford, X. Yung, K. Haller, J. Laane, G. Mestl, H. Knözinger, *J. Phys. Chem.* **1993**, *97*, 13810.
69. H. B. Zhang, G. D. Lin, H. L. Wan, Y. D. Liu, W. Z. Weng, J. X. Cai, Y. F. Shen, K. R. Tsai, *Catal. Lett.* **2001**, *73*, 141.
70. H. L. Wan, X. P. Zhou, W. Z. Weng, R. Q. Long, Z. S. Chao, W. D. Zhang, M. S. Chen, J. Z. Luo, S. Q. Zhou, *Catal. Today* **1999**, *51*, 161.
71. J. G. A. Pacheco, J. G. Eon, M. Schmal, *Catal. Lett.* **2000**, *68*, 197.
72. M. S. Palmer, M. Neurock, M. M. Olken, *J. Phys. Chem. B* **2002**, *106*, 6543.
73. M. S. Palmer, M. Neurock, M. M. Olken, *J. Am. Chem. Soc.* **2002**, *124*, 8452.
74. G. Gayko, D. Wolf, E. V. Kondratenko, M. Baerns, *J. Catal.* **1998**, *178*, 441.
75. E. V. Kondratenko, O. V. Buyevskaya, M. Soick, M. Baerns, *Catal. Lett.* **1999**, *63*, 153.
76. E. V. Kondratenko, D. Wolf, M. Baerns, *Catal. Lett.* **1999**, *58*, 217.
77. E. V. Kondratenko, O. V. Buyevskaya, M. Baerns, *J. Mol. Catal. A* **2000**, *158*, 199.
78. D. Wolf, M. Slinko, E. Kurkina, M. Baerns, *Appl. Catal. A* **1998**, *166*, 47.
79. M. Iwamoto, J. H. Lunsford, *J. Phys. Chem.* **1980**, *84*, 3079.
80. H. Borchert, M. Baerns, *J. Catal.* **1997**, *168*, 315.
81. A. Burrows, C. J. Kiely, G. J. Hutchings, R. W. Joyner, M. Y. Sinev, *J. Catal.* **1997**, *167*, 77.
82. A. Palermo, J. P. H. Vazquez, A. F. Lee, M. S. Tikhov, R. M. Lambert, *J. Catal.* **1998**, *177*, 259.
83. A. Burrows, C. J. Kiely, J. S. J. Hargreaves, R. W. Joyner, G. J. Hutchings, M. Y. Sinev, Y. P. Tulenin, *J. Catal.* **1998**, *173*, 383.
84. S. Bhatia, N. Zabidi, M. Ahmad, *React. Kinet. Catal. Lett.* **2001**, *74*, 87.
85. R. Spinicci, P. Marini, S. De Rossi, M. Faticanti, P. Porta, *J. Mol. Catal.* **2001**, *176*, 253.
86. Z. Zhang, X. E. Verykios, M. Baerns, *Catal. Rev. Sci. Eng.* **1994**, *36*, 507.
87. A. G. Anshits, E. N. Voskresenskaya, E. V. Kondratenko, N. G. Maksimov, *Catal. Today* **1995**, *24*, 217.
88. S. F. Ji, T. C. Xiao, S. B. Li, C. Z. Xu, R. L. Hou, K. S. Coleman, M. L. H. Green, *Appl. Catal. A* **2002**, *225*, 271.
89. S. F. Ji, T. C. Xiao, S. B. Li, L. J. Chou, B. Zhang, C. Z. Xu, R. L. Hou, A. P. E. York, M. L. H. Green, *J. Catal.* **2003**, *220*, 47.
90. S. F. Ji, T. C. Xiao, S. B. Li, L. J. Chou, B. Zhang, C. Z. Xu, R. L. Hou, M. L. H. Green, *Studies in Surface Science and Catalysis*, Vol. 147, Elsevier, Amsterdam, 2004, p. 607.
91. H. S. Chen, J. Z. Niu, B. Zhang, S. B. Li, *Acta Phys. Chim. Sin.* **2001**, *17*, 111.
92. E. V. Kondratenko, N. G. Maksimov, A. G. Anshits, *Kinet. Katal.* **1995**, *36*, 658.
93. A. J. Nagy, G. Mestl, R. Schlögl, *J. Catal.* **1999**, *188*, 58.
94. Y. S. Su, J. Y. Ying, W. H. Green, *J. Catal.* **2003**, *218*, 321.
95. D. Wolf, *Catal. Lett.* **1994**, *27*, 207.
96. D. Wolf, M. Heber, W. Grunert, M. Muhler, *J. Catal.* **2001**, *199*, 92.
97. M. M. Holena, M. Baerns, in *Handbook of Heterogeneous Catalysis*, 2nd Ed., G. Ertl, H. Knözinger, F. Schüth, J. Weitkamp (Eds.), Ch. 2.2, Wiley-VCH, Weinheim, 2008.
98. K. Huang, X. L. Zhan, F. Q. Chen, D. W. Lu, *Chem. Eng. Sci.* **2003**, *58*, 81.
99. E. Iwamatsu, K.-I. Aika, *J. Catal.* **1989**, *117*, 416.
100. L. Lehmann, M. Baerns, *J. Catal.* **1992**, *135*, 467.

101. Z. Stansch, L. Mleczko, M. Baerns, *Ind. Eng. Chem. Res.* **1997**, *36*, 2568.
102. C. T. Tye, A. R. Mohamed, S. Bhatia, *Chem. Eng. J.* **2002**, *87*, 49.
103. D. Schweer, L. Mleczko, M. Baerns, *Catal. Today* **1994**, *21*, 357.
104. I. P. Androulakis, S. C. Reyes, *AIChE. J.* **1999**, *45*, 860.
105. M. Baerns, W. Hinsen, US Patent 4 608 449, 1996.
106. A. V. Kruglov, M. C. Bjorklund, R. W. Carr, *Chem. Eng. Sci.* **1996**, *51*, 2945.
107. J. H. Edwards, K. T. Do, R. J. Tyler, p. 429–462, *Methane Conversion by Oxidative Processes, Fundamentals and Engineering Aspects*, E. E. Wolf (Ed.), Van Nostrand Reinhold, New York, 1992, p. 548.
108. L. Mleczko, M. Rothaemel, R. Andorf, M. Baerns, p. 487–494, in: Fluidization VII (O. E. Potters, D. J. Nicklin (Eds.)), American Institute of Chemical Engineers, New York, 1992, p.
109. U. Pannek, L. Mleczko, *Chem. Eng. Sci.* **1996**, *51*, 3537.
110. K. Kato, C. H. Wen, *Chem. Eng. Sci.* **1969**, *24*, 1351.
111. H. W. Zanthoff, M. Baerns, *Ind. Eng. Chem. Res.* **1990**, *29*, 2.
112. T. S. Pugsley, F. Berruti, *Chem. Eng. Sci.* **1996**, *51*, 2751.
113. U. Pannek, L. Mleczko, *Chem. Eng. Sci.* **1997**, *52*, 2429.
114. T. Nozaki, O. Yamazaki, K. Omata, *Chem. Eng. Sci.* **1992**, *47*, 2945.
115. Y. S. Lin, W. Wang, J. Han, *AIChE J.* **1994**, *40*, 786.
116. D. Lafarga, J. Santamaria, M. Menendez, *Chem. Eng. Sci.* **1994**, *49*, 2005.
117. J. Coronas, J. Santamaria, M. Menendez, *Chem. Eng. Sci.* **1994**, *49*, 2015.
118. D. Eng, M. Stoukides, *Catal. Rev. Sci. Eng.* **1991**, *33*, 375.
119. Y. K. Kao, L. Lei, Y. S. Lin, *Ind. Eng. Chem. Res.* **1997**, *36*, 3583.
120. Y. Zeng, Y. S. Lin, S. L. Swartz, *J. Membr. Sci.* **1998**, *150*, 87.
121. Y. Zeng, Y. S. Lin, *J. Catal.* **2000**, *193*, 58.
122. Y. Lu, A. G. Dixon, W. R. Moser, Y. H. Ma, U. Balachandran, *J. Membr. Sci.* **2000**, *170*, 27.
123. W. Kiatkittipong, T. Tagawa, S. Goto, S. Assabumrungrat, K. Silpasup, P. Praserthdam, *Chem. Eng. J.* **2005**, *115*, 63.
124. M. Baerns, L. Mleczko, H. Zanthoff, EU Research Project EN3C/0023-D, Bochum, 1991, p. 161.
125. K. R. Hall, *Catal. Today* **2005**, *106*, 243.
126. G. L. Culp, V. J. Stricker, J. R. Nelson, M. M. Bhasin, K. A. Nielsen, US Patent 6 518 476 B1, assigned to Union Carbide Chemicals & Plastics Technology Corporation, 2003.